Journal of Petroleum Science and Engineering 164 (2018) 571–583

Contents lists available at ScienceDirect

Journal of Petroleum Science and Engineering

journal homepage: www.elsevier.com/locate/petrol

Fluid flow in fractured reservoirs: Exact analytical solution for transient dual porosity model with variable rock matrix block size

Mahdi Abbasi [a], Mohammad Madani [b], Mohammad Sharifi [a,*], Alireza Kazemi [a]

[a] Department of Petroleum Engineering, Amirkabir University of Technology (Polytechnic of Tehran), P.O. Box: 15875-4413, Tehran, Iran
[b] Department of Petroleum Engineering, Ahwaz Faculty of Petroleum Engineering, Petroleum University of Technology (PUT), Ahwaz, Iran

ARTICLE INFO

Keywords:
Fractured reservoir
Transient dual-porosity model
Shape factor
Rock matrix block size distribution

ABSTRACT

Dual porosity reservoirs consist of two comparatively independent systems of fractures and matrix blocks with high and low permeability values, respectively. Semi-analytical and numerical studies on naturally fractured reservoirs have been already cited in the literature. The present study focuses on investigation of a linear double porosity model of a semi-infinite-acting naturally fractured reservoir using an exact analytical method. Different matrix block size distributions are embedded into a transient model to consider the effects of heterogeneity in fractured formations. In order to take into account transient fracture-matrix exchange, an analytical method is proposed to solve the coupled fracture and matrix equations. Gauss Legendre quadrature is employed to evaluate the double integral of general transient solution. Moreover, the corresponding shape factor was evaluated in a double porosity transient model coupled with variable matrix block size distribution. Results demonstrated that matrix block size distributions strongly affect the fluid transfer during the early time region. Also, the presented model was employed to generate interference test curves which in turn were studied to investigate the impacts of storativity ratio and matrix block size distributions on the fracture-matrix fluid transfer. Results illustrated that a series of obtained pressure data from an observational well along with the proposed model may be considered a robust method in fracture intensity assessment. Fast sensitivity analysis and very efficient computational cost are the benefit of the derived analytical solutions with respect to previous numerical solutions.

1. Introduction

More than half of the world remaining petroleum resources is left in naturally fractured reservoirs (NFRs) (Abdelazim and Rahman (2016)). It is believed that petroleum production from NFRs has widely met the universal requirements to nowadays energy demand (Sofla et al., 2016). Regarding the fact that naturally fractured reservoirs (NFRs) are intrinsically heterogenic at all scales, they have been known by researchers as one of the most difficult sorts of reservoirs to characterize; this may be attributed to their complex structure comprising two comparatively independent fracture and porous matrix systems. Such reservoirs are mathematically represented as single and double porosity models in the literature (Abbasi et al., 2017a; Golghanddashti, 2011; Jia et al., 2016; Narr, 2011; Nie et al., 2012; Rezaee, 2015; Wang et al., 2016; Wennberg et al., 2006).

In a typical NFR system, major flow paths into the wellbore are provided through the fracture system owing to their high usual reported permeability values of 0.5–2 Darcy while matrix porous volume is responsible for the main storativity due to their low typical permeability values of 0.1–2 mD (Saidi, 1987). In the literature, two distinguished analytical techniques of dual porosity models have been frequently cited for the mathematical description of flow behavior between fracture and matrix systems in NFRs, with the help of two partial differential equations; the first model assumes a pseudo-steady-state flow behavior, initially presented by Warren and Root (1963) and the second one assumes transient model, initially developed by Kazemi (1969) (Cornaton and Perrochet, 2002).

Warren and Root (1963) presented that there exists a direct proportional relationship between pressure difference of matrix-fracture systems and fluid flow transfer rate in a fully-linked, and regular fractured media. They incorporated two new factors as λ (inter-porosity flow coefficient) and ω (storativity coefficient) to indicate both system flow and storage capacities with the aim of NFR pressure response characterization. They were the first that utilized the advantageous Laplace transformation to solve the obtained dimensionless pressure function, which led to successfully presentation of a technique for pressure build-up data

* Corresponding author.
E-mail address: m_sharifi@aut.ac.ir (M. Sharifi).

https://doi.org/10.1016/j.petrol.2018.01.010
Received 20 February 2017; Received in revised form 10 December 2017; Accepted 4 January 2018
Available online 9 January 2018
0920-4105/© 2018 Published by Elsevier B.V.

Nomenclature

A	cross-sectional area open to flow, ft^2
a	exponential probability constant
b	fracture half-thickness, ft
c	Fluid compressibility, psi^{-1}
F_h	rock matrix block height ratio
g	intercept in the linear probability density function
k	absolute permeability, md
L_m	thickness of repetitive element, ft
L^{-1}	Laplace inverse
m	linear probability constant
p	pressure, psi
$\bar{\bar{p}}$	average pressure over the domain, psi
$\hat{p}$	pressure in the Laplace domain
q	production rate of fluid, bbl/day
s	Laplace space variable
t	time, seconds
x	matrix coordinate, ft
y	fracture coordinate, ft

Greek symbols

α	proportionality coefficient
ρ	fluid density, lb/ft^3
μ	fluid viscosity, cp
ω	storativity ratio
λ	interporosity flow coefficient
φ	porosity, fraction
σ	shape factor, ft^{-2}

Subscripts

D	dimensionless
f	fracture
i	initial
m	matrix
max	maximum
min	minimum
w	well

interpretation in infinite boundary radial reservoirs. Several researchers have extended Warren and Root model with special cases and assumptions since then (Bui et al., 2000; Da Prat et al., 1981; Mavor and Cinco-Ley, 1979; Odeh, 1965). For instance, presence of bounded outer boundary and constant pressure conditions at inner boundary for radial reservoir was introduced by Da Prat et al. (1981) for the first time which led to generation of characteristic type curve analysis for their assumptions; yet their results could not give satisfactory matching for actual field cases. Later, Bui et al. (2000) produced specific type curves to analyze the data adapted form pseudo steady state pressure response for partially penetrating wells in homogenous NFRs, which were useful in early and transition times.

Although transient-based models are much more mathematically complicated than pseudo-steady-state based models, they are substantially much more appealing due to consideration of all flow regimes including transient, late transient and pseudo-steady-state (Cornaton and Perrochet, 2002; Stewart, 2011). The initialization of pseudo steady state models in pressure response analysis dates back to 1969 when Kazemi (1969) utilized a uniform isotropic model having a slab matrix along with horizontal fractures to illustrate single phase fluid flow phenomenon in radial NFRs and then incorporated a numerical simulator to obtain the in-situ properties of reservoirs. He delineated that heterogeneity plays a key role in understanding pressure transient data analysis and further explained that two emerging parallel lines on semi-log graph could be ascribed to wellbore storage impacts and storativity parameter overestimation in case of no boundary effects. Later on, de Swaan O" (1976) investigated homogenous sphere and slab based matrix blocks in radial NFRs environment for the purpose of pressure distribution description assuming infinite boundary condition and with the help of heat flow theory. Fracture pressure was considered variable and a convolution term was incorporated to describe the source term. Based on their acquired results, early and late periods were identified by two parallel lines on semi-log plot. This model however failed to appropriately present the transition time between early and late periods. Cinco-Ley and Samaniego (1982) employed three new dimensionless parameters including fracture storativity, matrix hydraulic diffusivity, and fracture area to interpret pressure transient tests of radially slab and sphere shaped matrix blocks in NFRs. Based on their work, three characteristic flow regimes including fracture storage, transient matrix, and matrix pseudo steady state were detected. They also assessed the matrix geometry in NFRs in case of availability of smooth pressure data. Chen et al. (1985) proposed techniques to analyze drawdown and buildup pressure test data, assuming bounded cylindrical slab-based matrix blocks NFR alongside a constant rate producing well located at the center. They also modified MBH method to compute the average reservoir pressure for NFRs. Their results highlighted that five possible regimes could exist from which formation parameters can be calculated if the appropriate straight line is selected. Application of pressure transient response analysis for linear NFRs was initiated by El-Banbi (1998) for which he presented solutions assuming diverse inner and outer boundary conditions. The inner boundary conditions were considered as constant rate, constant well flowing rate, constant rate with wellbore storage and skin effect, and constant well flowing pressure with skin. The outer boundary conditions were infinite reservoir, closed reservoir, and constant pressure.

Shape factor is one of the controversial subjects which have been discussed in pressure response analysis cases, and is defined as an exchange coefficient in pseudo steady state based transfer equation, expressing fracture-matrix transfer. Shape factor was initially derived by Warren and Root (1963) for NFRs in a geometrical way. Derivation of Shape factors is based on pressure diffusion mechanism with the assumption of constant fracture pressure (Bourbiaux et al., 1999). Several researchers have devoted their works to obtain shape factors. Kazemi (1969) discretized the pressure equation, then applied the five point finite difference technique as a numerical simulator to obtain the shape factor in single phase double porosity systems. Bourbiaux et al. (1999) introduced a shape factor expression versus equivalent block dimension for two-dimensional fracture-matrix transfer formulation in double porosity simulators, assuming pseudo steady state condition. Hassanzadeh and Pooladi-Darvish (2006) stated that shape factors are boundary-conditional through the analytical solution of diffusivity equation in Laplace domain for several depletion schemes in the fracture.

Rock matrix block size is an important parameter in the naturally fractured reservoirs which has been investigated in the literature of pressure transient analysis (Braester, 1984). Braester introduced numerical solutions of pressure transient analysis for NFRs with ordered fracture-matrix blocks. He presented that homogenous behavior is observed in a relatively short time leading to disappearance of block size variation impacts in most feasible one-phase flow cases. Cinco-Ley et al. (1985) investigated the effects of multiple matrix block size distributions on behavior of pressure transient response in NFRs which resulted in a different observation of pressure derivative compared to Warren and Root model during only early times. Haddad et al. (2012) introduced the effects of variable matrix block size distribution on matrix-fracture mass transfer shape factor (during a tracer test) as a first order exchange coefficient. They highlighted that in fractured systems with small matrix block sizes, smaller dimensionless shape factor is observed during transient times. Haddad et al. (2014) introduced a mathematical model to explain the mass transfer phenomenon in fractured porous media considering two mechanisms of advective-dispersive transport within the fractures and diffusive transport within matrix blocks. They used several rock matrix block distributions to account for the effects of formation heterogeneity. They also explained that their developed model along with tracer data is an appropriate tool to assess the fracture intensity and dispersivity in fractured formations. Abbasi et al. (2017b) represented a heat transfer model for the process of cold water injection into fractured geothermal reservoirs in radial system and further explicated the dependency of heat transfer on matrix block size distribution.

The previous studies of linear fracture systems cited in the literature including El-Banbi (1998) and Bello (2009) have provided non-exact (semi-analytical) solutions. In addition, although some suggested shape factors have been developed for both transient and pseudo-steady state time regions (Hassanzadeh and Pooladi-Darvish, 2006), those have not been applied for pressure depletion in dual porosity models. More than that, the effect of matrix block size distribution on the developed shape factors (for pressure depletion) in above mentioned studies has not been considered.

In the present study and to the best knowledge of authors, for the first time pressure equation is solved in a single fracture model against spatial dimensions (x and y) and time using an exact analytical method based on conceptual fracture model assumptions and description.

For this purpose, diffusivity equation is initially transformed into Laplace space to calculate the both fracture and matrix block pressure at diverse locations and times. Afterwards, in a typical fluid transfer process, the corresponding dimensionless shape factor is obtained. To take into account the heterogeneity, effects of matrix block size distributions on the present analytical model are delineated, considering different fracture intensities. Moreover, unsteady state as well as pseudo steady state time regions in a typical fracture-matrix interaction are determined, based on the achieved derivation results. Finally, the presented model is employed to generate interference test curves which in turn are examined to investigate the impacts of storativity ratio and matrix block size distributions on the fracture-matrix fluid transfer.

2. Basic model

Warren and Root (1963) developed the conceptual double porosity systems in ideal fractured systems which is extensively utilized to describe pressure behavior in NFRs. The basic assumption of their work is on the basis of pseudo steady state matrix flow, wherein multiplication of average fracture-matrix pressure by shape factor value gives exchange flow rate extracted from reservoir matrix. de Swaan O" (1976) introduced another double porosity system in which a set of equally-spaced and parallel fractures make the matrix media and matrix/fracture systems are related to each other via an unsteady state exchange term. The developed physical model here is demonstrated in Fig. 1. Following terms are assumed to describe the conceptual model: an isotropic and homogenous matrix, constant matrix and fracture permeability, slightly compressible fluid of the formation, isothermally single-phase oil flow. It is noteworthy that the exchange flow only occurs from reservoir matrix into the fracture.

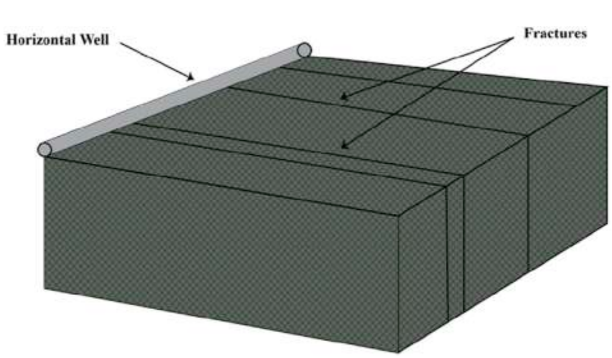

Fig. 1. The schematic representation of a horizontal penetrated production well into a fractured reservoir.

3. Mathematical model

The analytical model introduced in the present study is structurally demonstrated in Fig. 2. The matrix block which has an initial pressure of P_i, is surrounded by a pair of parallel fractures noted with a smaller pressure of P_f which can be obtained through the solution of diffusivity equation in the fracture system. It should be stated that pressure diffusion occurs from the matrix block center point to the fracture system, leading to a zero value in the matrix center and equal matrix surface-fracture pressure values.

3.1. Governing equations for fluid flow

One can obtain the governing fracture fluid flow differential equation by considering the control volume in the fracture and using the material balance rule. The derivation process is identical to those offered by several authors as discussed through equation (A1) to (A8) in the Appendix (Bello, 2009; Brohi et al., 2011; El-Banbi, 1998; Fujiwara, 1989).

The fracture-based equation is defined as (El-Banbi, 1998):

$$\left(\frac{\varphi\mu c_t}{k}\right)_f \frac{\partial p_f}{\partial t} - \frac{\partial^2 p_f}{\partial y^2} - \frac{2k_m}{k_f L_m}\frac{\partial p_m}{\partial x}\bigg|_{x=b} = 0 \tag{1}$$

Where in fracture and rock matrix fluid pressure are denoted by p_f and p_m, respectively. Other notations have been explained in the nomenclature. The governing 1-dimensional fluid flow equation of rock matrix pressure distribution is as follows:

$$\left(\frac{\varphi\mu c_t}{k}\right)_m \frac{\partial p_m}{\partial t} - \frac{\partial^2 p_m}{\partial x^2} = 0 \tag{2}$$

The followings are the boundary and initial conditions:

$$p_f(y,0) = p_m(y,x,0) = p_i \tag{3a}$$

$$p_f(0,t) = p_w \tag{3b}$$

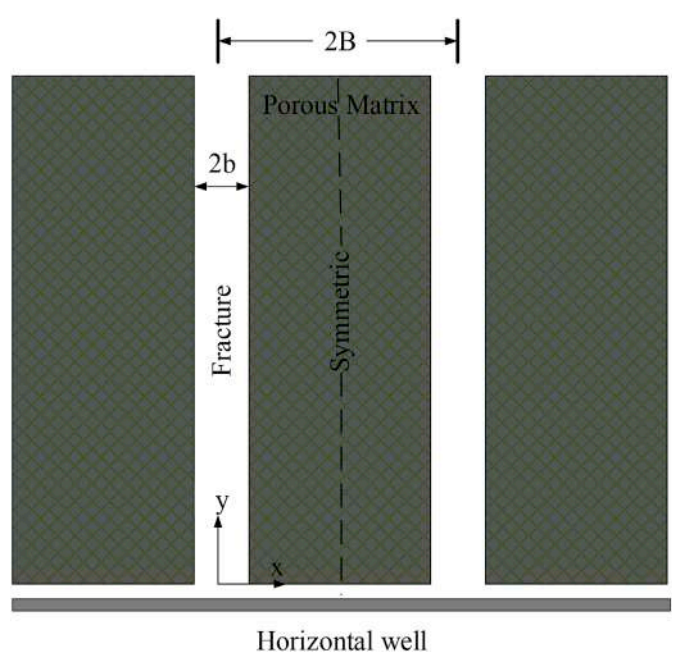

Fig. 2. Basic representation of developed analytical model.

$$p_f(y\to\infty,t)=p_i \tag{3c}$$

$$p_f(y,t)=p_m(y,b,t) \tag{3d}$$

$$p_{Dm}=\frac{4\lambda}{3\sqrt{\pi}(1-\omega)}\int_l^{\infty}\exp(-\xi^2).\int_0^{\infty}\frac{1}{\varepsilon}\exp(\varepsilon_R)\sum_{n=0}^{\infty}(-1)^n(2n+1).\cos\left[\frac{(2n+1)\pi x_D}{2}\right]$$
$$\cdot\left[\begin{array}{l}\dfrac{1}{\dfrac{\varepsilon^4}{4}+\left(\dfrac{\pi^2\lambda(2n+1)^2}{12(1-\omega)}\right)^2}\left\{\begin{array}{l}\left(\dfrac{\pi^2\lambda(2n+1)^2}{12(1-\omega)}\sin(\varepsilon_I)|_T-\dfrac{\varepsilon^2}{2}\cos(\varepsilon_I)|_T\right)\\ +\exp\left[-\left(\dfrac{\pi^2\lambda(2n+1)^2}{12(1-\omega)}\right)t_D\right].\left[\left(\dfrac{\pi^2\lambda(2n+1)^2}{12(1-\omega)}\right)\sin(\Omega')+\dfrac{\varepsilon^2}{2}\cos(\Omega')\right]\end{array}\right\}\\ +\left(\dfrac{12(1-\omega)}{\pi^2\lambda(2n+1)^2}\right)\left[1-\exp\left[-\left(\dfrac{\pi^2\lambda(2n+1)^2}{12(1-\omega)}\right)t_D\right]\right]\sin(\Omega)\end{array}\right]d\varepsilon d\xi \tag{9}$$

$$\left.\frac{\partial p_m}{\partial x}\right|_{x=B}=0 \tag{3e}$$

Here, dimensionless parameters are employed to reduce the complications involved in this study. Governing equations may be placed in their dimensionless forms through exploitation of dimensionless parameters as below:

Therefore, one can derive the boundary conditions and dimensionless diffusivity equations noted below. Based on the dimensionless pressure and dimensionless production relationship, one may simply obtain:

$$q_D=-\frac{1}{2\pi}\left.\frac{\partial p_{Df}}{\partial y_D}\right|_{y_D=0} \tag{4}$$

Substitution of dimensionless variables in Eqs. (1) and (2) gives:

For fracture:

$$\omega\frac{\partial p_{Df}}{\partial t_D}-\frac{\partial^2 p_{Df}}{\partial y_D^2}-\frac{\lambda}{3}\left.\frac{\partial p_{Dm}}{\partial x_D}\right|_{x_D=\frac{2b}{L_m}}=0 \tag{5}$$

For matrix:

$$\frac{3}{\lambda}(1-\omega)\frac{\partial p_{Dm}}{\partial t_D}-\frac{\partial^2 p_{Dm}}{\partial x_D^2}=0 \tag{6}$$

Also, initial and boundary conditions become:

$$p_{Df}(y_D,0)=p_{Dm}(y_D,x_D,0)=0 \tag{7a}$$

$$p_{Df}(0,t_D)=1 \tag{7b}$$

$$p_{Df}(y_D\to\infty,t_D)=0 \tag{7c}$$

$$p_{Df}(y_D,t_D)=p_{Dm}\left(y_D,\frac{2b}{L_m},t_D\right) \tag{7d}$$

$$\left.\frac{\partial p_{Dm}}{\partial x_D}\right|_{x_D=\frac{2B}{L_m}}=0 \tag{7e}$$

Solutions of Eqs. (5) and (6) are given in Appendix, which have been solved at the boundary and initial conditions by applying the Laplace transform. Due to the difficulties associated with numerical inversion, the solutions used are based on analytical inversion of the Laplace transform. Eqs. (8) and (9) express the dimensionless pressure distribution in a fracture and porous matrix:

$$p_{Df}=\frac{4}{\pi^{3/2}}\int_l^{\infty}\exp(-\xi^2).\int_0^{\infty}\frac{1}{\varepsilon}\exp(\varepsilon_R)\left[\sin(\varepsilon_I)|_T+\sin(\Omega)\right]d\varepsilon d\xi \tag{8}$$

Eq. (9) represents matrix dimensionless pressure. In order to find average matrix pressure, one can integrate Eq. (9) which yields:

$$\overline{p}_{Dm}=\frac{1}{V_m}\int_{V_m}p_{Dm}dV_m \tag{10}$$

As mentioned, in the pseudo steady state period, there exists a direct proportional relationship between pressure difference of matrix-fracture systems and fluid flow transfer rate; this proportionality coefficient is known as the shape factor (σ), defined in:

$$q_m=\frac{k_m\rho}{\mu}\sigma\left(\overline{p_m}-p_f\right) \tag{11}$$

Moreover, the matrix-fracture fluid flow can be derived as a function of matrix pressure, as stated in the following equation:

$$q_m=-\phi_m c_m\rho\frac{\partial\overline{p}_m}{\partial t} \tag{12}$$

Combining Eqs. (11) and (12) gives:

$$\frac{k_m\rho}{\mu}\sigma=\phi_m c_m\rho\frac{\partial\overline{p}_{Dm}/\partial t}{\left(p_{Df}-\overline{p_{Dm}}\right)} \tag{13}$$

Now we can utilize the solution of the diffusivity equation to obtain matrix pressure considering its boundary and initial conditions. With the help of these equations, one may derive shape factor as follows:

$$\sigma=\frac{(\varphi c_t)_m}{\left[(\varphi c_t)_m+(\varphi c_t)_f\right]A}\frac{k_f}{k_m}\frac{\partial\overline{p}_{Dm}/\partial t_D}{(p_{Df}-\overline{p}_{Dm})} \tag{14}$$

According to the dimensionless parameters defined in Table 1, dimensionless shape factor (σL_m^2) can be obtained by substitution of fracture half thickness (b) in terms of the dimensionless length as:

$$\sigma L_m^2=\frac{12(1-\omega)}{\lambda}\frac{\partial\overline{p}_{Dm}/\partial t_D}{(p_{Df}-\overline{p}_{Dm})} \tag{15}$$

4. Results and discussion

In this section, solution for Eq. (A.1) and (A.2), which are derived for the introduced conceptual model and presented in Fig. 2, is described. Fracture linear flow, fracture linear to fracture/matrix bilinear transition

Table 1
Dimensionless parameters used to derive dimensionless governing equations.

Parameters	Equation
Dimensionless time	$t_D = \frac{0.00633 k_f t}{[(\varphi c_t)_m + (\varphi c_t)_f]\mu A}$
Dimensionless pressure	$p_D = \frac{p_i - p}{p_i - p_w}$
Dimensionless production	$q_D = \frac{k_f \sqrt{A}(p_i - p_w)}{141.2 q B \mu}$
Storativity ratio	$\omega = \frac{[\varphi c_t]_f}{[\varphi c_t]_m + [\varphi c_t]_f}$
Interporosity flow coefficient	$\lambda = \alpha \frac{k_m}{k_f} A;\ \alpha = \frac{12}{L_m^2}$
Dimensionless length	$x_D = \frac{x}{L_m/2}; y_D = \frac{y}{\sqrt{A}}$

flow, and fracture to matrix linear flow are believed to strongly depend on the storativity ratio (ω). In the early time, most of the production is from the fracture system due to its high permeability. According to ω definition, the fracture to matrix storage ratio, the more the fracture porosity, the more the fluid-in-place is within the fracture system and more oil production in the early time accordingly. Moreover, in a fractured reservoir with low ω values (matrix and fracture system are highlighted with high and low porosity, respectively), low oil production occurs in the early time due to low matrix porosity, which is accompanied by comparatively high oil production as time passes due to matrix-to-fracture oil transfer phenomenon.

It is notable that fracture linear flow is altered into fracture pseudo steady state flow, followed by matrix linear flow at large ω values; however, fracture linear flow to fracture/matrix bilinear flow is the flow regime alteration at small ω values. Impact of ω on the proposed solution is illustrated in Fig. 3 at a fixed value of $\lambda = 10^{-3}$.

Parameters such as matrix per fracture permeability ratio and matrix block width affect the value of interporosity flow coefficient (λ). Fig. 4 demonstrates impact of interporosity flow coefficient on the solution at a constant value of ω = 0.01. It should be expressed that interporosity flow coefficient also controls the fracture pseudo steady state flow regime (also known as transition state from fracture to matrix linear flow regime), which in turn affects matrix linear to matrix pseudo steady state flow. Also, owing to existence of direct and inverse proportionality of λ with matrix permeability and matrix-squared width, respectively, matrix pseudo steady state flow regime starts at later times for smaller λ values.

4.1. Uniform rock matrix block size distribution (Warren and Root model)

Warren and Root (1963) extended the work of Barenblatt et al. (1960) and found out a relationship among fluid mobility, potential difference, fracture-matrix exchange term, and shape factor. For the purpose of modeling solute transport and fluid flow in double porosity systems, the

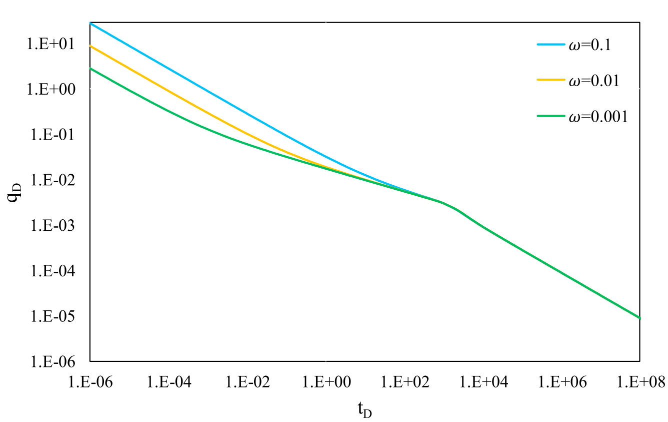

Fig. 3. Impact of storativity ratio (ω) on the developed solution. At early times, the more the storativity ratio causes the higher dimensionless rate, as the oil production is mostly from the fracture. At late time however, all three cases give the same dimensionless rate, since matrix is the main storage contributor to the oil production.

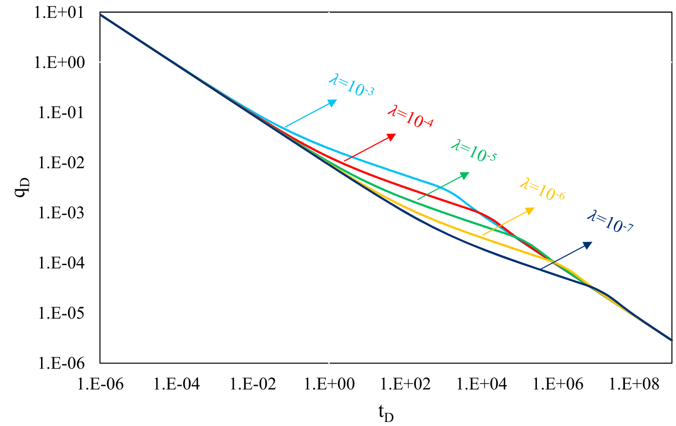

Fig. 4. Impact of interporosity coefficient (λ) on the developed solution (when ω = 0.01). At early times, because the oil production is mostly from the fracture, a change in the interporosity coefficient does not affect the dimensionless rate. However, when the matrix starts to contribute to oil production, the matrix with higher permeability (i.e., higher interporosity coefficient) comes with relatively larger dimensionless rate.

pseudo steady state model which is also known as a first-order matrix--fracture exchange relationship, has been utilized. In the present paper, it is assumed that fracture-matrix fluid flow is proportional to fracture fluid pressure variation with time.

Fig. 5 demonstrates dimensionless shape factors for different values of $y_D = 0.1$, $y_D = 10$ and $y_D = 100$ at a fixed value of $\omega = 0.03$ and $\lambda = 10^{-3}$, leading to two major physical scenarios; locations near the injection point (i.e., small y_D values) and locations far away from the injection point (i.e., large y_D values). Also, Fig. 5 highlights two characteristic time regions in terms of dimensionless shape factor; transient period during which shape factor is a function of time and pseudo steady state period during which dimensionless shape factor does not change with time. Based on Fig. 5, one can conclude that for the first scenario, (i.e., $y_D = 0.1$ or $y_D = 10$), and second scenario (i.e., $y_D = 100$), the value of dimensionless shape factor approaches π^2 and 12 during pseudo steady state time region, respectively. Also, longer transient time region occurs in the second scenario of fluid flow, which means that a time relay in the matrix blocks response exist far from the producer source. In such a case, longer transients exist owing to variation of fracture fluid pressure which acts as a matrix block boundary condition with respect to time. In the first fluid flow scenario however, shorter transients are observed because of constant fracture fluid pressure (Dirichlet-type boundary). Such results have also been noted by Haddad et al. (2012) for tracer tests in dual porosity systems for an injection well assuming wellbore concentration is

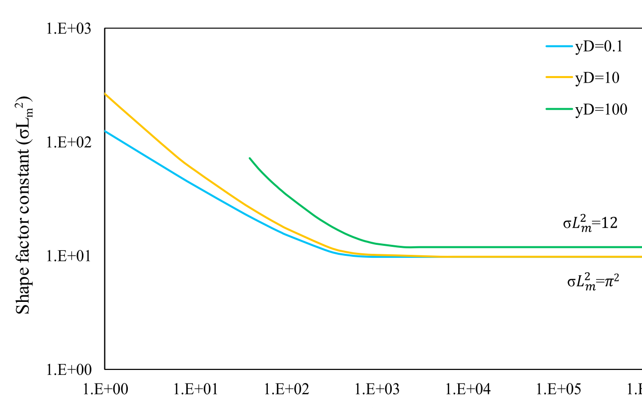

Fig. 5. Effect of dimensionless distance (y_D) on dimensionless shape factor versus dimensionless time.

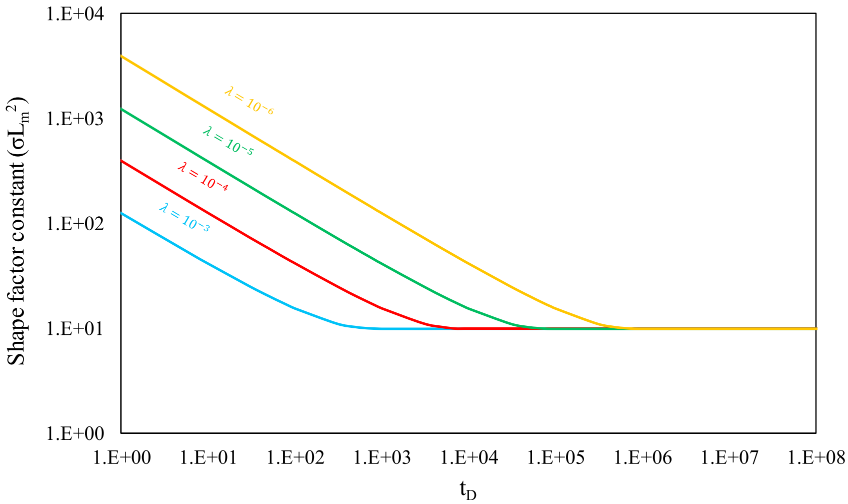

Fig. 6. Effect of interporosity flow coefficient (λ) on the dimensionless shape factor against dimensionless time (when ω = 0.03).

Table 2
Rock and fluid properties (Kazemi, 1969).

Parameters	$\varnothing_m$	$\varnothing_f$	$L_m/2$	b	k_m	k_f	c_m	c_f	P_i	P_w	μ
Value	0.05	0.45	9.05	0.025	0.01	7236.39	10^{-5}	10^{-5}	4000	1500	1
Unit	%	%	ft	ft	md	md	psi^{-1}	psi^{-1}	psi	psi	cp

constant.

The λ coefficient used in the presented formulation, represents fracture storage coefficient to that of the matrix block. In order to investigate the impact of fracture storage coefficient to that of the matrix block on dimensionless shape factor separately, the interporosity coefficient was changed considering constant values of $\omega = 0.03$ and $y_D = 0.1$. Fig. 6 indicates that the more the fracture-matrix shape factor in transition time, the less the value of λ coefficient, and also the dimensionless shape factor eventually stabilizes at π^2 no matter what the value of λ coefficient is.

The presented analytical model was validated against numerical Kazemi's model (Kazemi, 1969). For this purpose, a Cartesian model was defined using a commercial simulator considering the following assumptions: 1- Single-phase fluid. 2- Linear flow inside the fracture and a perpendicular flow over the fracture linear flow inside the matrix. 3- The fracture is horizontal. 4- The matrix and fracture are both isotropic and homogeneous. Table 2 tabulates the rock and fluid properties as the input to the simulator.

Moreover, Fig. 7 demonstrates the schematic grid formatted in Cartesian coordinate.

Fig. 8 shows the semi-log plot of bottom-hole pressure as a function of time, which highlights that the analytical model presented in this study is in very good agreement with the simulator results. The advantageous point to mention here is that the analytical model run time is much lesser compared to the simulator. Therefore, the analytical model is more appropriate than the numerical model in preliminary assessments and sensitivity analyses (see Table 3).

Table 3
Probability distribution function (Rafael et al., 2001).

Distribution	Probability Density Function (PDF)	Parameters	
Exponential	$f_D(L_{mD}) = \frac{a\ \exp(-L_{mD})}{\exp(-aF_h)-\exp(-a)}$	$a = -20$, $-5, 5, 20$	Represent highly sparse to highly intense fractured systems
Linear	$f_D(L_{mD}) = mL_{mD} + g$	$g = \frac{2-m(F_h^2)}{2(1-F_h)}$	$m > 0$: low fracture density $m = 0$: rectangular distribution $m < 0$: high fracture density

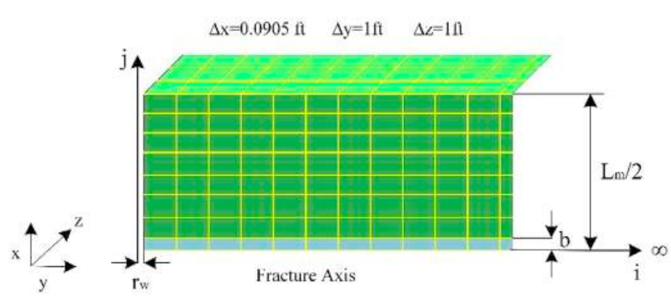

Fig. 7. The schematic simulation grid formatted in Cartesian coordinate.

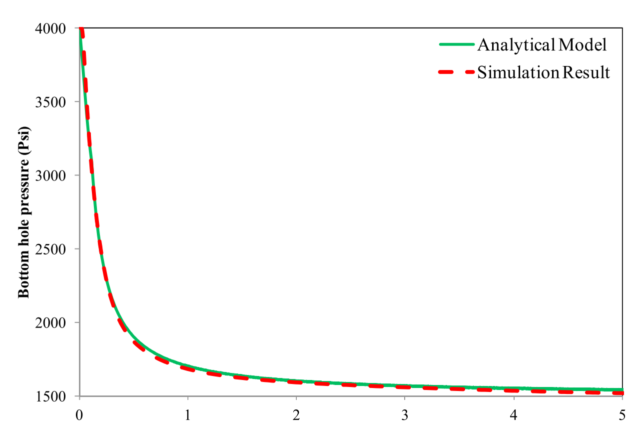

Fig. 8. Plot of bottom-hole pressure versus time.

4.2. Effect of rock matrix block size distribution

The results discussed in the previous subsection were based on the assumption of a uniform matrix block size (Warren and Root model). Due to heterogeneity of real geological formations, there exists a different range of rock matrix block sizes. This necessitates the reformulation of the problem to account for variation of rock matrix block size distributions in the naturally fractured rocks. Exponential and linear distributions are the most probable distributions of rock matrix blocks that can be observed in outcrops (Neretnieks, 2002; Segall, 1981). Geological studies of fractured reservoirs and outcrops have shown non-uniformity in fracture spacing due to different lithology and other geotechnical effects (Reis, 1998). It should be noted that pressure transient analysis with rock matrix block size distribution has been addressed in many studies (Rafael et al., 2001; Rodriguez-N- et al., 2002) (see Fig. 9).

$$\frac{\partial \overline{\overline{p_{Dm}}}}{\partial t_D} = L^{-1}\left\{\int_{F_h}^{1} \frac{a\exp(-aL_m)}{\exp(-aF_h)-\exp(-a)} \frac{1}{\sqrt{\frac{(1-\omega)k_f(L_{m\max}L_m)^2 s}{4k_mA}}} \tanh\left(\sqrt{\frac{(1-\omega)k_f(L_{m\max}L_m)^2 s}{4k_mA}}\right) \times \exp\left(-\left[\omega s + \sqrt{\frac{4Ak_m(1-\omega)s}{(L_{m\max}L_m)^2 k_f}} \tanh\left(\sqrt{\frac{(1-\omega)k_f(L_{m\max}L_m)^2 s}{4k_mA}}\right)\right]^{1/2} y_D\right) dL_m\right\} \tag{18}$$

$$\sigma\overline{\overline{L_m}}^2 = \frac{2L^{-1}\left\{\int_{F_h}^{1} \frac{a\exp(-aL_m)}{\exp(-aF_h)-\exp(-a)} \sqrt{\frac{(1-\omega)k_f(L_{m\max}L_m)^2}{k_mAs}} \tanh\left(\sqrt{\frac{(1-\omega)k_f(L_{m\max}L_m)^2 s}{4k_mA}}\right) \exp\left(-\left[\omega s + \sqrt{\frac{4Ak_m(1-\omega)s}{(L_{m\max}L_m)^2 k_f}} \tanh\left(\sqrt{\frac{(1-\omega)k_f(L_{m\max}L_m)^2 s}{4k_mA}}\right)\right]^{1/2} y_D\right) dL_m\right\}}{L^{-1}\left\{\int_{F_h}^{1} \frac{a\exp(-aL_m)}{\exp(-aF_h)-\exp(-a)} \frac{1}{s}\left[1-\frac{1}{\sqrt{\frac{(1-\omega)k_f(L_{m\max}L_m)^2 s}{4k_mA}}} \tanh\left(\sqrt{\frac{(1-\omega)k_f(L_{m\max}L_m)^2 s}{4k_mA}}\right)\right] \exp\left(-\left[\omega s + \sqrt{\frac{4Ak_m(1-\omega)s}{(L_{m\max}L_m)^2 k_f}} \tanh\left(\sqrt{\frac{(1-\omega)k_f(L_{m\max}L_m)^2 s}{4k_mA}}\right)\right]^{1/2} y_D\right) dL_m\right\}} \tag{19}$$

A probability density function (PDF) has the following property (Rafael et al., 2001):

$$\int_{F_h}^{1} f_D(L_{mD})dL_{mD} = 1 \tag{16}$$

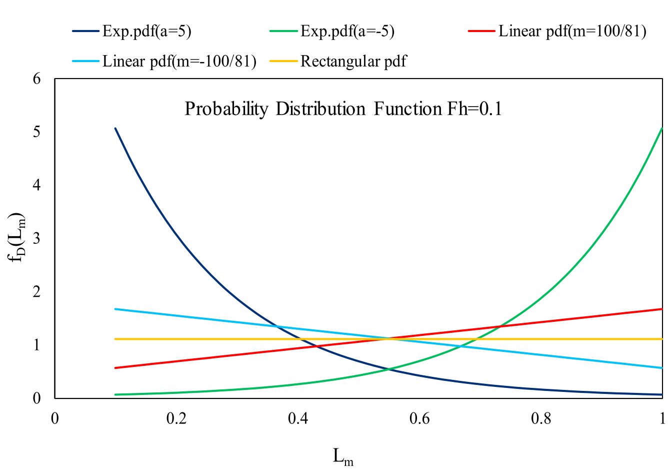

Fig. 9. Graphical representation of linear, rectangular and exponential distributions against $L_{mD} = L_m/L_{m\max}$ (Haddad et al., 2012).

where $f_D(L_{mD})$ is the probability density function and $L_{mD} = L_m/L_{m\max}$. The linear and exponential forms of probability density functions and their corresponding parameters are indicated in Table 3.

Where $F_h = L_{m\min}/L_{m\max}$. In this study, a value of 0.1 for F_h is used (Johns and Jalali, 1991; Rafael et al., 2001).

$$\overline{\overline{p_{Dm}}} = \int_{F_h}^{1} f_D(L_m)\overline{p}_{Dm}dL_m \tag{17}$$

For an exponential distribution, the term $\frac{\partial \overline{\overline{p_{Dm}}}}{\partial t_D}$ is:

Therefore, using Eq. (15), the dimensionless shape factor with an exponential rock matrix block size distribution can be expressed by:

For other distributions, the same procedure must be followed. In calculation of the dimensionless shape factor using Eq. (19), numerical instabilities may arise at high values of y_D. In such a case, Eq. (15) can be used to calculate the dimensionless shape factor by replacing L_m with $\hat{L}_m$. A sensitivity analysis reveals that the dimensionless shape factors obtained by this replacement are close to those obtained using Eq. (19).

Fig. 10 shows the dimensionless shape factor for all possible distributions considered in this study for $y_D = 0.1$ and $\omega = 0.01$, wherein it can be observed that as the fracture intensity increases (increase in small rock matrix blocks, i.e., from $L_m = 10$ft towards 100ft), the dimensionless shape factor (σL_m^2) decreases. In addition, as increase in fracture intensity leads to reduction in the time needed to reach pseudo steady state. This corresponds to shorter transients and earlier onset of the pseudo steady-state period for very small rock matrix blocks.

Fig. 10 shows that the dimensionless shape factor demonstrates a transient behavior at early time and converges to a stabilized value during the pseudo steady state period. This behavior has been observed for pressure transient analysis in dual porosity systems (Chang, 1995; Hassanzadeh and Pooladi-Darvish, 2006; Ranjbar et al., 2011).

Fig. 11 shows the matrix pressure of several exponential distributions of matrix block size. As parameter a increases from negative to positive values, i.e., as the fracture intensity increases, the matrix-fracture exchange increases, which in turn causes the oil production from matrix block to boost. One can therefore conclude that in exponential distribution of matrix block size, the value of parameter a holds a direct

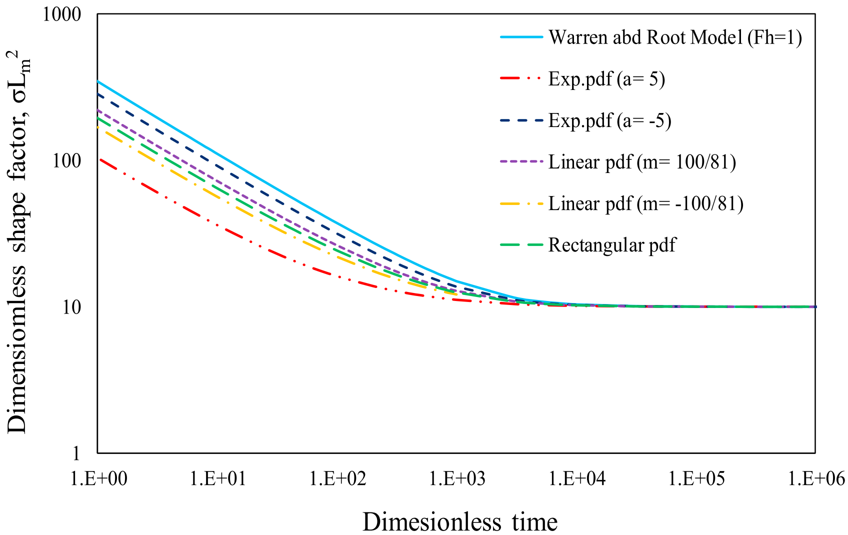

Fig. 10. Impact of matrix block size distributions on the dimensionless shape factor with respect to dimensionless time.

relationship with both matrix oil production and the imposed pressure drop at a specified time.

Fig. 12 illustrates the pressure derivative as a function of time, which also implies that an increase in the fracture intensity raises the matrix oil production rate and matrix pressure drop.

The linear matrix block size distribution was initially introduced by

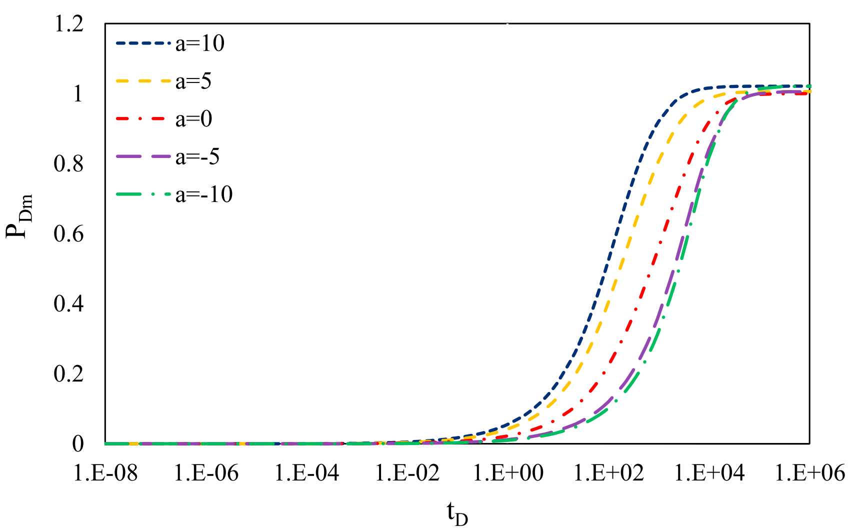

Fig. 11. Impact of several exponential PDFs of matrix block size on the dimensionless matrix pressure against dimensionless time in an observational well located at a linear distance of $y_D = 0.1$ with $\omega = 0.01$.

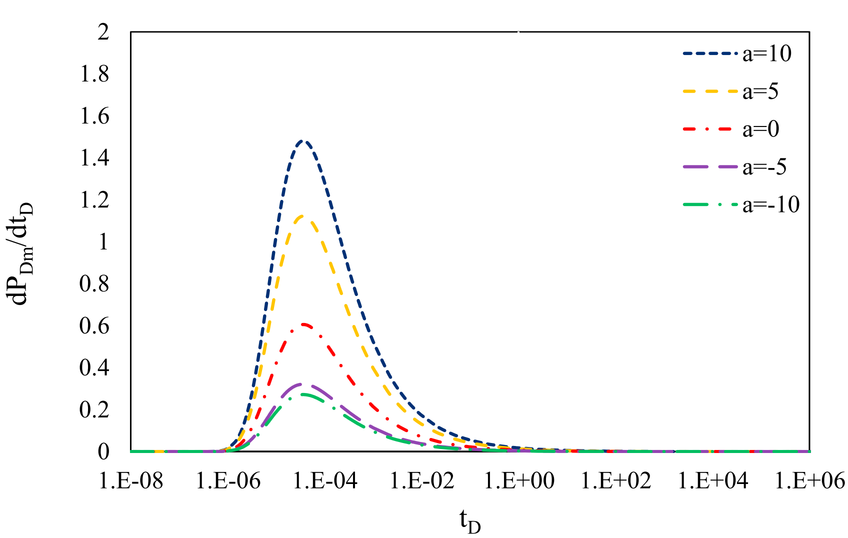

Fig. 12. Impact of several exponential PDFs of matrix block size on the dimensionless matrix pressure derivative against dimensionless time in an observational well at a linear distance of $y_D = 0.1$ with $\omega = 0.01$.

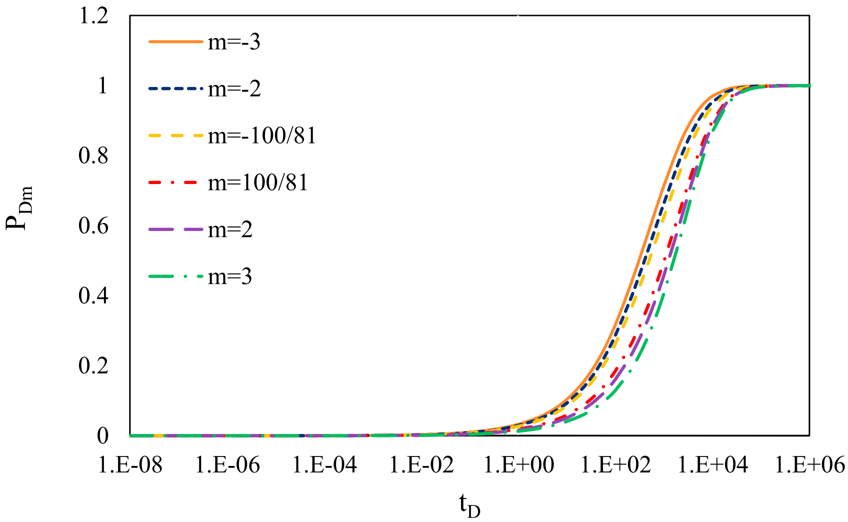

Fig. 13. Impact of several linear PDFs of matrix block size on the dimensionless matrix pressure versus dimensionless time in an observational well at a linear distance of $y_D = 0.1$ with $\omega = 0.01$.

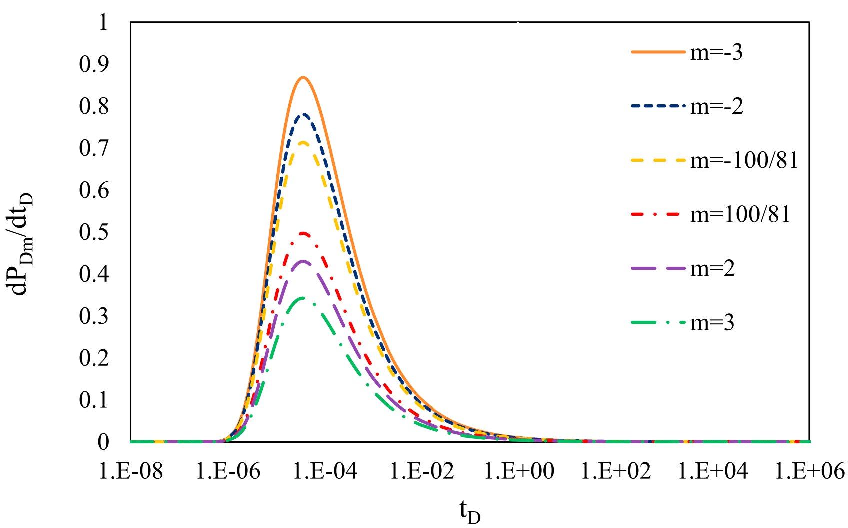

Fig. 14. Impact of several exponential PDFs of matrix block size on the dimensionless matrix pressure derivative against dimensionless time in an observational well at a linear distance of $y_D = 0.1$ with $\omega = 0.01$.

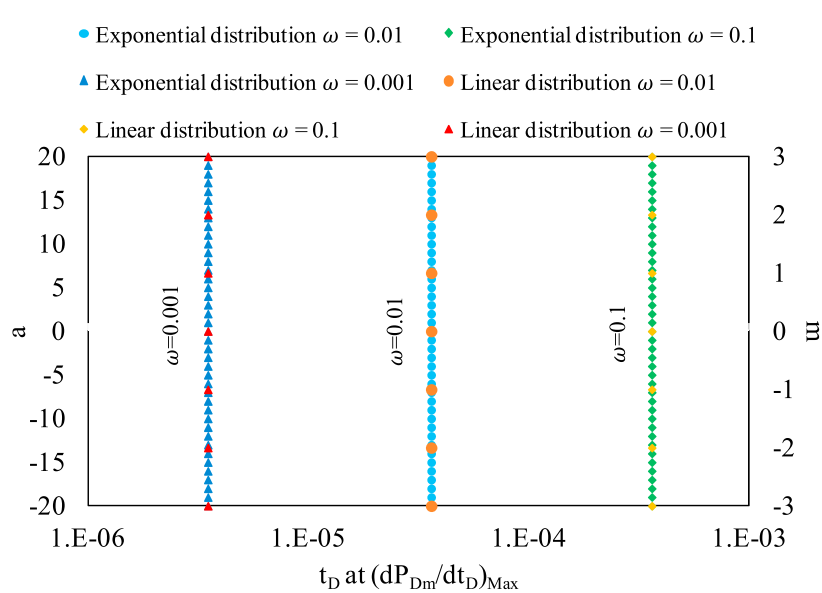

Fig. 15. Dimensionless time associated with the maximum derivative of the tracer concentration profile in diverse linear and exponential PDFs in an observational well at a linear distance of $y_D = 0.1$, considering different storativity ratio.

Rodriguez et al. (Rodriguez-N- et al., 2002); Effect of such linear distribution on dimensionless shape factor is conceptually represented in Fig. 13. As parameter *m* decreases from positive to negative values, i.e., as the fracture intensity increases, the matrix-fracture exchange increases, which in turn causes the oil production from matrix block to boost. One can therefore conclude that in linear distribution of matrix block size, the value of parameter *m* is inversely related with both matrix oil production and the imposed pressure drop at a specified time.

Fig. 14 illustrates the pressure derivative as a function of time, which also implies that an increase in the fracture intensity raises the matrix oil production rate and matrix pressure drop.

The dimensionless time associated with the maximum dimensionless matrix pressure derivative is presented in Fig. 15 for the cases of linear and exponential probability density functions (PDFs), from which one can conclude that location of maximum derivative is almost not dependable on matrix block size distribution type. Therefore, pressure derivative analysis may be considered as a unique feature as opposed to pressure analysis.

Considering the fact that dimensionless drainage radius at the maximum changing value of matrix block pressure is simply an indicator of pressure drop arrival to observational well (Bourdet, 2002), and also since the fracture system consists of high permeable zones, therefore, pressure drop approaches the observational well through the fracture system. It can be concluded that type of matrix block distribution does not affect pressure drop arrival time. This behavior has been observed for tracer test analysis in fractured systems (Haddad et al., 2014) where they utilized the behavior seen in the derivative plot of tracer concentration to assess the dispersivity in the observational well. Their results implied the non-dependency of dispersivity on rock matrix block size distribution in fractures where dispersive transport is dominated.

Fig. 15 also illuminates that fracture storage coefficient is directly proportional with the value of ω and that pressure drop arrives faster to the production well as ω decreases (fracture storativity is smaller).

5. Conclusions

In this study, an accurate analytical solution was developed to examine the transient fracture-matrix exchange in a typical semi-infinite-acting naturally fractured reservoir. Heterogeneity of fractured reservoirs was considered in terms of exponential and linear matrix block size distributions. Results implied the strong dependency of fluid exchange on matrix block size distribution throughout early time.

The pressure transient analysis indicates that boundary condition influences the pseudo steady state dimensionless shape factor in the sense that at locations near and far away the injection source, the pseudo steady state dimensionless shape factor reaches around π^2 and 12, respectively. The transient shape factor in this study which is developed as a function of matrix block size distribution, can be incorporated as a matching parameter in the history matching process.

The effect of matrix block size distributions such as linear and exponential, and storativity ratio on the radius of investigation was investigated by analyzing the pressure response in the observational well through the interference test. Based on the investigation, pressure drop arrived the observational well through the fracture system in the interference test of naturally fractured reservoirs and matrix block size distribution type did not affect this pressure drop arriving time.

Acknowledgements

The authors greatly acknowledge the support and guidance provided by the staff of Nargan Amitis Energy Development Company.

Appendix

Fracture and average matrix block pressure are calculated in this section over Laplace domain, by applying Laplace transform on Eqs. (5) and (6). To begin the derivation process, taking Laplace transformation with respect to t_D, Eqs. (5) and (6) are respectively converted to:

$$\frac{\partial^2 \hat{p}_{Df}}{\partial y_D^2} - \omega s \hat{p}_{Df} + \frac{\lambda}{3}\frac{\partial \hat{p}_{Dm}}{\partial x_D}\bigg|_{x_D=\frac{2b}{L_m}} = 0 \tag{A.1}$$

$$\frac{\partial^2 \hat{p}_{Dm}}{\partial x_D^2} - \frac{3}{\lambda}(1-\omega)s\hat{p}_{Dm} = 0 \tag{A.2}$$

Note that fracture and rock matrix dimensionless pressure are denoted by $\hat{p}_{Df}$ and $\hat{p}_{Dm}$, respectively, in the Laplace domain, in which the boundary conditions (Eq. (7b) - (7e)) become:

$$\hat{p}_{Df}(0) = \frac{1}{s} \tag{A.3a}$$

$$\hat{p}_{Df}(y_D \to \infty) = 0 \tag{A.3b}$$

$$\hat{p}_{Df}(y_D) = \hat{p}_{Dm}\left(r_D, \frac{2b}{L_m}\right) \tag{A.3c}$$

$$\frac{\partial \hat{p}_{Dm}}{\partial x_D}\bigg|_{x_D=\frac{2B}{L_m}} = 0 \tag{A.3d}$$

The general solution transform of $\hat{p}_{Dm}$for the ordinary differential equation of Eq. (A.2) is derived as:

$$\hat{p}_{Dm} = C_1 \cosh\left(\sqrt{\frac{3(1-\omega)s}{\lambda}}\left(\frac{2B}{L_m} - x_D\right)\right) + C_2 \sinh\left(\sqrt{\frac{3(1-\omega)s}{\lambda}}\left(\frac{2B}{L_m} - x_D\right)\right) \tag{A.4}$$

In which *s* is the Laplace space variable. The second boundary condition defined in Eq. (A.3d) provides $C_2 = 0$ and considering first boundary condition defined in Eq. (A.3c), Eq. (A.4) becomes:

$$\hat{p}_{Dm} = \frac{\cosh\left(\sqrt{\frac{3(1-\omega)s}{\lambda}}\left(\frac{2B}{L_m} - x_D\right)\right)}{\cosh\left(\sqrt{3(1-\omega)s/\lambda}\right)}\hat{p}_{Df} \tag{A.5}$$

Now, in order to find the dimensionless fracture pressure, partial differential equation defined in Eq. (A.1) is solved at a constant value of $x_D = \frac{2b}{L_m}$ to get:

$$\left.\frac{\partial \hat{p}_{Dm}}{\partial x_D}\right|_{x_D=\frac{2b}{L_m}} = -\hat{p}_{Df}\sqrt{\frac{3(1-\omega)s}{\lambda}}\tanh\left(\sqrt{\frac{3(1-\omega)s}{\lambda}}\right) \tag{A.6}$$

Substituting Eq. (A.6) into Eq. (A.1) gives:

$$\frac{\partial^2 \hat{p}_{Df}}{\partial y_D^2} - \left\{\omega s + \sqrt{\frac{\lambda(1-\omega)s}{3}}\tanh\left(\sqrt{\frac{3(1-\omega)s}{\lambda}}\right)\right\}\hat{p}_{Df} = 0 \tag{A.7}$$

Eq. (A.7), which is an ordinary differential equation (ODE), is solved, then using the boundary conditions presented by Eq. (A.3b) and (A.3c), following term is derived for $\hat{p}_{Df}$:

$$\widehat{p}_{Df} = \frac{1}{s}\exp\left(-\left[\omega s + \sqrt{\frac{\lambda(1-\omega)s}{3}}\tanh\left(\sqrt{\frac{3(1-\omega)s}{\lambda}}\right)\right]^{1/2} y_D\right) \tag{A.8}$$

Now, inverse Laplace transformation must be applied on Eq. (A.8). For the matter of simplicity, the following integral is utilized in the derivation process (Grandshteyn and Ryzhik, 1980):

$$\int_0^\infty \exp\left(-\xi^2 - \frac{\chi^2}{\xi^2}\right)d\xi = \frac{\sqrt{\pi}}{2}\exp(-2\chi) \tag{A.9}$$

This integral (Eq. (A.9)) is employed to convert Eq. (A.7) into the following form:

$$\widehat{p}_{Df} = \frac{2}{\sqrt{\pi}s}\int_0^\infty \exp(-\xi^2)\exp\left(-\frac{\left[\omega s + \sqrt{\frac{\lambda(1-\omega)s}{3}}\tanh\left(\sqrt{\frac{3(1-\omega)s}{\lambda}}\right)\right]}{4\xi^2}y_D^2\right) \tag{A.10}$$

We can rewrite Eq. (A.10) to:

$$\widehat{p}_{Df} = \frac{2}{\sqrt{\pi}}\int_0^\infty \exp(-\xi^2)\frac{1}{s}exp\left(-\frac{\omega y_D^2}{4\xi^2}s\right)\exp\left(-\frac{y_D^2}{4\xi^2}\sqrt{\frac{\lambda(1-\omega)s}{3}\tanh\left(\sqrt{\frac{3(1-\omega)s}{\lambda}}\right)}\right) \tag{A.11}$$

Therefore, the inverse transform is used to give the dimensionless fracture pressure as:

$$p_{Df} = \frac{2}{\sqrt{\pi}}\int_0^\infty \exp(-\xi^2)\int_0^T L^{-1}\left[\exp\left(-\frac{y_D^2}{4\xi^2}\sqrt{\frac{\lambda(1-\omega)s}{3}}\tanh\left(\sqrt{\frac{3(1-\omega)s}{\lambda}}\right)\right)\right]_\tau d\tau d\xi \tag{A.12}$$

In which, T is defined as:

$$T = t_D - \frac{\omega y_D^2}{4\xi^2} \quad T \geq 0$$

Note that Eq. (A.12) was obtained considering:

$$L^{-1}\left[\frac{1}{s}\exp(-as)f(s)\right] = \int_0^{t-a} L^{-1}[f(s)]d\tau \quad t > a \tag{A.13a}$$

$$L^{-1}\left[\frac{1}{s}\exp(-as)f(s)\right] = 0 \quad t < a \tag{A.13b}$$

The inverse of exponential term presented in Eq. (A.12) has been already discussed in Skopp and Warrick (1974) work, where a model was developed to describe reactive solutes in soil. Their inverse technique is applied here:

$$L^{-1}\left\{\exp\left(-\frac{y_D^2}{4\xi^2}\sqrt{\frac{\lambda(1-\omega)s}{3}}\tanh\left(\sqrt{\frac{3(1-\omega)s}{\lambda}}\right)\right)\right\} = \frac{1}{\pi}\int_0^\infty \varepsilon \exp(\varepsilon_R)\cos(\varepsilon_I)\, d\varepsilon \tag{A.14}$$

Wherein ε_R and ε_I are defined as:

$$\varepsilon_R = -\frac{y_D^2\varepsilon}{8\xi^2}\sqrt{\frac{\lambda(1-\omega)}{3}}\left(\frac{\sinh\left(\sqrt{3(1-\omega)/\lambda}\varepsilon\right) - \sin\left(\sqrt{3(1-\omega)/\lambda}\varepsilon\right)}{\cosh\left(\sqrt{3(1-\omega)/\lambda}\varepsilon\right) + \cos\left(\sqrt{3(1-\omega)/\lambda}\varepsilon\right)}\right)$$

$$\varepsilon_I = \frac{\varepsilon^2 t_D}{2} - \frac{y_D^2 \varepsilon}{8\xi^2}\sqrt{\frac{\lambda(1-\omega)}{3}}\left(\frac{\sinh\left(\sqrt{3(1-\omega)/\lambda}\varepsilon\right)+\sin\left(\sqrt{3(1-\omega)/\lambda}\varepsilon\right)}{\cosh\left(\sqrt{3(1-\omega)/\lambda}\varepsilon\right)+\cos\left(\sqrt{3(1-\omega)/\lambda}\varepsilon\right)}\right)$$

Substituting Eq. (A.14) in Eq. (A.12), then switching the integration order of τ and ε gives:

$$p_{Df} = \frac{4}{\pi^{3/2}}\int_0^\infty \exp(-\xi^2).\int_0^\infty \frac{1}{\varepsilon}\exp(\varepsilon_R)\left[\sin(\varepsilon_I)|_T + \sin(\Omega)\right] d\varepsilon d\xi \tag{A.15}$$

where

$$\Omega = \frac{y_D^2 \varepsilon}{8\xi^2}\sqrt{\frac{\lambda(1-\omega)}{3}}\left(\frac{\sinh\left(\sqrt{3(1-\omega)/\lambda}\varepsilon\right)+\sin\left(\sqrt{3(1-\omega)/\lambda}\varepsilon\right)}{\cosh\left(\sqrt{3(1-\omega)/\lambda}\varepsilon\right)+\cos\left(\sqrt{3(1-\omega)/\lambda}\varepsilon\right)}\right)$$

The requirements of above equation are:

$$t_D \geq \frac{\omega y_D^2}{4\xi^2} \text{ or } \xi \geq \frac{y_D}{2}\sqrt{\frac{\omega}{t_D}}$$

Hence, the final form of Eq. (A.15) is given as:

$$p_{Df} = \frac{4}{\pi^{3/2}}\int_l^\infty \exp(-\xi^2).\int_0^\infty \frac{1}{\varepsilon}\exp(\varepsilon_R)\left[\sin(\varepsilon_I)|_T + \sin(\Omega)\right] d\varepsilon d\xi \tag{A.16}$$

Where

$$l = \frac{y_D}{2}\sqrt{\frac{\omega}{t_D}}$$

is the integration lower limit versus ξ. Eq. (A.16) represents fracture dimensionless pressure considering all possible processes.

Solution for the dimensionless matrix pressure is now presented. Knowing the fact that inverse of the hyperbolic cosine function in Eq. (A.5) becomes (Badii and Oberhettinger (1973)):

$$L^{-1}\left\{\frac{\cosh\left(\sqrt{\frac{3(1-\omega)s}{\lambda}}\left(\frac{2B}{L_m}-x_D\right)\right)}{\cosh\left(\sqrt{3(1-\omega)s/\lambda}\right)}\right\} = \frac{\pi\lambda}{3(1-\omega)}\sum_{n=0}^\infty(-1)^n(2n+1).\exp\left[-\left(\frac{\pi^2\lambda(2n+1)^2}{12(1-\omega)}\right)t\right].\cos\left[\frac{(2n+1)\pi x_D}{2}\right] \tag{A.17}$$

In convolution theorem, it is stated that:

$$L^{-1}[f_1(p)f_2(p)] = \int_0^t F_1(\tau)F_2(t-\tau)d\tau \tag{A.18}$$

Therefore, the inverse of Eq. (A.17) can be written as:

$$p_{Dm} = \frac{\pi\lambda}{3(1-\omega)}\sum_{n=0}^\infty(-1)^n(2n+1).\cos\left[\frac{(2n+1)\pi x_D}{2}\right]\int_0^{t_D} p_{Df}(y_D,\tau)\exp\left[-\left(\frac{\pi^2\lambda(2n+1)^2}{12(1-\omega)}\right)(t-\tau)\right]d\tau \tag{A.19}$$

By replacing Eq. (A.16) in Eq. (A.19) for p_{Dm}, the following is obtained by integrating Eq. (A.19) with respect to τ:

$$\begin{aligned} p_{Dm} = &\frac{4\lambda}{3\sqrt{\pi}(1-\omega)}\int_l^\infty \exp(-\xi^2).\int_0^\infty \frac{1}{\varepsilon}\exp(\varepsilon_R)\sum_{n=0}^\infty(-1)^n(2n+1).\cos\left[\frac{(2n+1)\pi x_D}{2}\right] \\ &.\left[\begin{array}{l} \frac{1}{\frac{\varepsilon^4}{4}+\left(\frac{\pi^2\lambda(2n+1)^2}{12(1-\omega)}\right)^2}\left\{\begin{array}{l}\left(\frac{\pi^2\lambda(2n+1)^2}{12(1-\omega)}\sin(\varepsilon_I)|_T - \frac{\varepsilon^2}{2}\cos(\varepsilon_I)|_T\right) \\ +\exp\left[-\left(\frac{\pi^2\lambda(2n+1)^2}{12(1-\omega)}\right)t_D\right].\left[\left(\frac{\pi^2\lambda(2n+1)^2}{12(1-\omega)}\right)\sin(\Omega')+\frac{\varepsilon^2}{2}\cos(\Omega')\right]\end{array}\right\} \\ +\left(\frac{12(1-\omega)}{\pi^2\lambda(2n+1)^2}\right)\left[1-\exp\left[-\left(\frac{\pi^2\lambda(2n+1)^2}{12(1-\omega)}\right)t_D\right]\right]\sin(\Omega) \end{array}\right]d\varepsilon d\xi \end{aligned} \tag{A.20}$$

where

$$\Omega' = \Omega + \frac{\omega y_D^2 \varepsilon^2}{8\xi^2}$$

References

Abbasi, M., Izadmehr, M., Karimi, M., Sharifi, M., Kazemi, A., 2017a. Analytical study of fluid flow modeling by diffusivity equation including the quadratic pressure gradient term. Comput. Geotech. 89, 1–8.

Abbasi, M., Khazali, N., Sharifi, M., 2017b. Analytical model for convection-conduction heat transfer during water injection in fractured geothermal reservoirs with variable rock matrix block size. Geothermics 69, 1–14.

Abdelazim, R., Rahman, S.S., 2016. Estimation of permeability of naturally fractured reservoirs by pressure transient analysis: an innovative reservoir characterisation and flow simulation. J. Petrol. Sci. Eng. 145.

Badii, L., Oberhettinger, F., 1973. Tables of Laplace Transforms. Sprlnger-Verlag.

Barenblatt, G., Zheltov, I.P., Kochina, I., 1960. Basic concepts in the theory of seepage of homogeneous liquids in fissured rocks [strata]. J. Appl. Math. Mech. 24 (5), 1286–1303.

Bello, R.O., 2009. Rate Transient Analysis in Shale Gas Reservoirs with Transient Linear Behavior. Texas A&M University.

Bourbiaux, B., et al., 1999. Scaling up matrix-fracture transfers in dual-porosity models: theory and application. In: SPE Annual Technical Conference.

Bourdet, D., 2002. Well Test Analysis (Handbook of Petroleum Exploration and Production). Elsevier Science, Amsterdam.

Braester, C., 1984. Influence of block size on the transition curve for a drawdown test in a naturally fractured reservoir. Soc. Petrol. Eng. J. 24 (05), 498–504.

Brohi, I.G., Pooladi-Darvish, M., Aguilera, R., 2011. Modeling fractured horizontal wells as dual porosity composite reservoirs-application to tight gas, shale gas and tight oil cases. In: Presented at SPE Western North American Region Meeting, Alaska, USA, May 7–11.

Bui, T., Mamora, D., Lee, W., 2000. Transient pressure analysis for partially penetrating wells in naturally fractured reservoirs. In: Presented at the 2000 SPE Rocky Mountain Regional/Low-permeability Reservoirs Symposium and Exhibition, Colorado, Mar. 12–15.

Chang, M.M., 1995. Analytical Solution to Single and Two-phase Flow Problems of Naturally Fractured Reservoirs: Theoretical Shape Factor and Transfer Functions. PhD dissertation. The University of Tulsa.

Chen, C.-C., Serra, K., Reynolds, A.C., Raghavan, R., 1985. Pressure transient analysis methods for bounded naturally fractured reservoirs. Soc. Petrol. Eng. J. 25 (03), 451–464.

Cinco-Ley, H., Samaniego, V., 1982. Pressure transient analysis for naturally fractured reservoirs. In: Presented at the 57th SPE Annual Technical Conference and Exhibition, LA, Sept. 26–29.

Cinco-Ley, H., Samaniego, V., Kucuk, F., 1985. The pressure transient behavior for naturally fractured reservoirs with multiple block size. In: Presented at the 60th SPE Annual Technical Conference and Exhibition, LV, Sept. 22–25.

Cornaton, F., Perrochet, P., 2002. Analytical 1D dual-porosity equivalent solutions to 3D discrete single-continuum models. Application to karstic spring hydrograph modelling. J. Hydrol. 262 (1), 165–176.

Da Prat, G., Cinco-Ley, H., Ramey Jr., H., 1981. Decline curve analysis using type curves for two-porosity systems. Soc. Petrol. Eng. J. 21 (03), 354–362.

de Swaan O, A., 1976. Analytic solutions for determining naturally fractured reservoir properties by well testing. Soc. Petrol. Eng. J. 16 (03), 117–122.

El-Banbi, A.H., 1998. Analysis of Tight Gas Well Performance. Texas A&M University.

Fujiwara, K., 1989. Rate Decline Analysis for Naturally Fractured Reservoirs. Stanford University.

Golghanddashti, H., 2011. A new analytically derived shape factor for gas–oil gravity drainage mechanism. J. Petrol. Sci. Eng. 77 (1), 18–26.

Grandshteyn, I., Ryzhik, I., 1980. Table of Integrals, Series, and Products. Academic, New York.

Haddad, A.S., Hassanzadeh, H., Abedi, J., 2012. Advective–diffusive mass transfer in fractured porous media with variable rock matrix block size. J. Contam. Hydrol. 133, 94–107.

Haddad, A.S., Hassanzadeh, H., Abedi, J., Chen, Z., 2014. Application of tracer injection tests to characterize rock matrix block size distribution and dispersivity in fractured aquifers. J. Hydrol. 510, 504–512.

Hassanzadeh, H., Pooladi-Darvish, M., 2006. Effects of fracture boundary conditions on matrix-fracture transfer shape factor. Transport Porous Media 64 (1), 51–71.

Jia, P., Cheng, L., Huang, S., Wu, Y., 2016. A semi-analytical model for the flow behavior of naturally fractured formations with multi-scale fracture networks. J. Hydrol. 537, 208–220.

Johns, R., Jalali, Y., 1991. Comparison of pressure-transient response in intensely and sparsely fractured reservoirs. SPE Form. Eval. 6 (04), 513–518.

Kazemi, H., 1969. Pressure transient analysis of naturally fractured reservoirs with uniform fracture distribution. Soc. Petrol. Eng. J. 9 (04), 451–462.

Mavor, M.J., Cinco-Ley, H., 1979. Transient pressure behavior of naturally fractured reservoirs. In: Presented at the 1979 SPE California Regional Meeting, California, Apr. 18–20.

Narr, W., 2011. Characterization of Naturally Fractured Reservoirs.

Neretnieks, I., 2002. A stochastic multi-channel model for solute transport—analysis of tracer tests in fractured rock. J. Contam. Hydrol. 55 (3), 175–211.

Nie, R.-S., et al., 2012. Dual porosity and dual permeability modeling of horizontal well in naturally fractured reservoir. Transport Porous Media 92 (1), 213–235.

Odeh, A., 1965. Unsteady-state behavior of naturally fractured reservoirs. Soc. Petrol. Eng. J. 5 (01), 60–66.

Rafael, R.-N., Heber, C.-L., Heber, C.-L., Fernando, S.-V., Fernando, S.-V., 2001. A variable block size model for the characterization of naturally fractured reservoirs. In: Presented at the SPE Annual Technical Conference and Exhibition, Louisiana, 30 Sept.-3 Oct.

Ranjbar, E., Hassanzadeh, H., Chen, Z., 2011. Effect of fracture pressure depletion regimes on the dual-porosity shape factor for flow of compressible fluids in fractured porous media. Adv. Water Resour. 34 (12), 1681–1693.

Reis, J.C., 1998. Effect of fracture spacing distribution on pressure transient response in naturally fractured reservoirs. J. Petrol. Sci. Eng. 20 (1), 31–47.

Rezaee, R., 2015. Fundamentals of Gas Shale Reservoirs. John Wiley & Sons.

Rodriguez, N.R., Cinco, L.H., Samaniego, V.F., 2002. Fractured reservoir parameters estimation considering multiple block size. In: Presented at SPE International Petroleum Conference and Exhibition, Mexico, Feb. 10–12.

Saidi, A.M., 1987. Reservoir Engineering of Fractured Reservoirs: Fundamental and Practical Aspects. Total.

Segall, P., 1981. The Development of Joints and Faults in Granitic Rocks [Ph. D. thesis]. Stanford University, Stanford, California.

Skopp, J., Warrick, A., 1974. A two-phase model for the miscible displacement of reactive solutes in soils. Soil Sci. Soc. Am. J. 38 (4), 545–550.

Sofla, S.J.D., Pouladi, B., Sharifi, M., Shabankareian, B., Moraveji, M.K., 2016. Experimental and simulation study of gas diffusion effect during gas injection into naturally fractured reservoirs. J. Nat. Gas Sci. Eng. 33, 438–447.

Stewart, G., 2011. Well Test Design & Analysis. PennWell Corporation.

Wang, J., Xu, J., Wang, Y., Li, H., 2016. A new production predicting model of fractured horizontal wells in dual-porosity gas reservoirs on non-Darcy flow conditions. J. Petrol. Sci. Eng. 146, 670–676.

Warren, J., Root, P.J., 1963. The behavior of naturally fractured reservoirs. Soc. Petrol. Eng. J. 3 (03), 245–255.

Wennberg, O., et al., 2006. Fracture intensity vs. mechanical stratigraphy in platform top carbonates: the Aquitanian of the Asmari Formation, Khaviz Anticline, Zagros, SW Iran. Petrol. Geosci. 12 (3), 235–246.